Available online at www.sciencedirect.com

ScienceDirect

Ceramics International 39 (2013) 9237–9245

CERAMICS INTERNATIONAL

www.elsevier.com/locate/ceramint

Alkali-activated blends of calcium aluminate cement and slag/diatomite

K. Arbi*, A. Palomo, A. Fernández-Jiménez

Instituto Eduardo Torroja (CSIC), 28033 Madrid, Spain

Received 22 January 2013; received in revised form 3 May 2013; accepted 9 May 2013
Available online 21 May 2013

Abstract

The present study deals with the formulation of new cementitious materials via the alkaline activation of an industrial by-product (blast furnace slag) or a natural rock (diatomite) in the presence of reactive aluminium sourced from calcium aluminate cement (CAC). Two blends, one containing 20% CAC and 80% slag and the other 20% CAC and 80% diatomite, were prepared and activated with sodium sulphate or a sodium hydroxide solution. The hardened materials were characterised with X-ray diffraction (XRD) as well as ^{27}Al and ^{29}Si nuclear magnetic resonance (NMR) and tested for their 2-day mechanical strength. The main reaction product was a cementitious gel that precipitated with crystalline phases such as ettringite, U phase and katoite. While the slag blend reacted to generate a C–(A)–S–H-like gel under moderately alkaline conditions, diatomite reactivity proved to be very low under such conditions. The greater reactivity of both slag and diatomite at high pH (high alkalinity) favoured their interaction with CAC.

Keywords: Alkaline activation; Geopolymer; Calcium aluminate cement (CAC); Slag; Diatomite

1. Introduction

Since the entry into effect of the Kyoto protocols (1997), the cement industry, which is estimated to account for 6–7% of world-wide CO_2 emissions [1], has made earnest attempts to modernise cement manufacture and design alternative binders, primarily to improve energy efficiency and reduce polluting emissions. One of the avenues being explored is the alkali activation of aluminosilicates found in nature or industrial waste (such as metakaolin, fly ash and slag) [2–10]. Although such binders have been under study since the 1950s [11], it was not until the 1990s that cementitious systems based on the alkaline activation of aluminosilicates became a research target for teams the world over [12–19].

More specifically, calcium- and silicon-rich materials (SiO_2+CaO > 70%) such as blast furnace slag are being explored with particular intensity in an attempt to develop a new generation of binders based on alkaline activation technology [20–23]. The chemical interaction between slag and alkaline solutions (NaOH, KOH, $M_2O \cdot SiO_3 \cdot nH_2O$ (M=Na, K), Na_2CO_3) triggers a series of reaction mechanisms (dissolution, nucleation, condensation and precipitation) and ultimately the formation of cementitious products. These calcium silicate hydrates are similar to the gel obtained during Portland cement hydration [23,24], but with a small amount of Al in their structure (C–(A)–S–H gel). The cohesive properties of this latter gel largely explain the strength and durability of the materials obtained by alkali-activating slag.

Given its amorphous silica content, diatomite holds potential for the cement industry. Nonetheless, most of the studies conducted to date address its microstructural characterisation [25–28], its use in brick manufacture [29] or, more recently, the possible application of diatomite–limestone blends as a base binder in concrete [30,31].

At this time, alkaline cements are the object of in-depth study, for many unknowns relating to the mechanisms that govern the activation of the materials involved are yet to be clarified. Further research is also needed on the nature of the hydration products formed, their interaction with activating

*Corresponding author. Tel.: +34 913020440.
E-mail addresses: kamel@ietcc.csic.es, rbikml@gmail.com (K. Arbi).

0272-8842/$ - see front matter © 2013 Elsevier Ltd and Techna Group S.r.l. All rights reserved.
http://dx.doi.org/10.1016/j.ceramint.2013.05.031

substances and the mechanical behaviour of the resulting cements. Prior studies have shown that the main product of the alkaline activation of aluminosilicates is an aluminosilicate gel (typically N–A–S–H gel [3,4]), and that aluminium, which links silica tetrahedra, plays a key role during gel formation (especially in the initial stages of the reaction) [32,33] and hence the need for a minimum amount of reactive aluminium in the starting materials to guarantee the formation of N–A–S–H gel and with it, satisfactory strength development in the cement obtained. As a reactive aluminium-bearing material, CAC is a constituent of promise for future formulations [34,35]. Depending on the alkalinity and silicon content in the starting materials, CAC hydration may be governed by the usual or other mechanisms [36,37].

The present study focuses on the formulation of new cementitious materials by alkali-activating blends compositionally located in the $CaO/SiO_2/Al_2O_3$ ternary system, and more specifically blends M1=(20% CAC+80% BFS) and M2=(20% CAC+80% diatomite). The microstructure of the cement matrices is analysed with XRD as well as ^{27}Al and ^{29}Si NMR to acquire a deeper understanding of the mechanisms that govern alkaline activation in this type of CAC-containing systems.

2. Experimental procedure

The calcium aluminate cement (CAC) used in this study was furnished by Molins SA, Spain, while the blast furnace slag (BFS) and diatomite were sourced from South America. The experimental procedure began by mixing two blends of prime materials in the following proportions: M1=(20% CAC+80% BFS) and M2=(20% CAC+80% diatomite). The experimental design required the two binders to have similar Al_2O_3 contents but different CaO/SiO_2 and Al_2O_3/SiO_2 ratios. The chemical composition of the starting materials (CAC, BFS and diatomite) and working blends are given in Table 1.

Both blends were alkali-activated with a low alkalinity solid activator (6% Na_2SO_4) and a high pH liquid (8 M NaOH solution). The cement pastes were prepared with different liquid/solid ratios for each binder–activator combination to obtain similar consistencies. They were subsequently moulded into $10 \times 10 \times 60\ mm^3$ prismatic specimens for curing in a chamber at 99% relative humidity. The specimens were removed from the moulds after 24 h and stored in the chamber until they reached the test age (2 days).

Bending and compressive strength were determined by testing the specimens to failure on an Ibertest Autotest 200/10-SW test frame.

The hardened materials were finely ground and submerged in acetone and ethanol to stop the hydration reactions prior to XRD mineralogical and NMR microstructural characterisation.

The chemical composition of the starting materials (Table 1) was found with X-ray fluorescence (XRF) on a Bruker S8 TIGER wavelength dispersive X-ray fluorescence spectrometer, with a 4-kW, 60-kV, 170-mA intermediate power X-ray generator. LiF 220, LiF 200, PET and XS-55 analyser crystals were used with 0.2- and 0.3-mm Cu as well as 0.8-, 0.2-, 0.5-, 0.1- and 0.0125-mm Al filters.

The samples were analysed on a Bruker D8 ADVANCE X-ray diffractometer with a high voltage 4-kW generator, a 40-kV, 30-mA copper anode X-ray tube, an automatic divergence slit, a graphite monochromator and an automatic sample changer. In most cases the patterns were recorded in a 5–60° 2θ interval at a rate of 0.01973° per 0.5 s.

The nuclear magnetic resonance spectra were obtained at ambient temperature on a Bruker Avance 400 (9.4 T) spectrometer. The resonance frequency settings were 104.26 MHz (^{27}Al) and 79.49 MHz (^{29}Si). The ^{29}Si MAS-NMR spectra ($I=1/2$) were recorded by irradiating the sample with a $\pi/2$ (4-μs) pulse, using a 500-kHz filter. The analogous pulse and filter settings for the ^{27}Al ($I=3/2$) MAS-NMR spectra were $\pi/8$ (1.5-μs) and 100-kHz and 2-MHz, respectively.

Table 1
Chemical analysis of the starting materials and working blends.

Constituent	CAC	BFS	Diatomite	M1	M2
SiO_2	3.46	37.42	66.98	30.63	54.28
Al_2O_3	42.6	11.47	4.94	17.70	12.47
Fe_2O_3	14.93	0.66	2.10	3.514	4.67
MnO	0.02	0.19	0.01	0.15	0.012
MgO	0.38	10.62	1.16	8.57	1.00
CaO	35.8	32.71	3.34	33.33	9.83
SO_3	0.08	2.96	1.16	2.38	0.94
Na_2O	–	1.47	2.32	1.17	1.86
K_2O	0.10	1.19	0.88	0.97	0.72
TiO_2	1.65	0.50	0.23	0.73	0.51
P_2O_5	0.07	0.05	0.62	0.05	0.51
Cl	–	–	2.04	–	1.63
Other	0.91	0.76	0.80	0.79	0.82
Loss on ignition	0.61	0.77	13.42	0.74	10.90
Total	100	100	100	100	100
Al_2O_3/SiO_2	12.31	0.30	0.07	0.58	0.23
CaO/SiO_2	10.31	0.87	0.05	1.08	0.18

Table 2
Compositions, liquid/solid ratios, densities and bending and compressive strengths in the 2-day blends analysed.

Blend	Composition (%, mass)	Activator	L/S ratio	Density (g m^{-3})	Strength (MPa)	
					Bending	Compressive
$M1_{NS}$	20% CAC+80% BFS	Na_2SO_4 (6%)	0.35[a]	2.01 ± 0.2	3.37 ± 0.2	10.73 ± 0.5
$M1_{NH}$	20% CAC+80% BFS	NaOH (8M)	0.5[b]	1.94 ± 0.01	2.40 ± 0.40	23.67 ± 2.5
$M2_{NS}$	20% CAC+80% diatomite	Na_2SO_4 (6%)	0.72[a]	1.37 ± 0.03	0.53 ± 0.07	2.51 ± 0.1
$M2_{NH}$	20% CAC+80% diatomite	NaOH (8M)	0.85[b]	1.64 ± 0.09	0.45 ± 0.05	1.21 ± 0.08

[a] The liquid used was water.
[b] An 8 M NaOH solution.

Scanning electron microscopy (SEM) was deployed primarily to confirm some of the possible interpretations of the data generated by the aforementioned techniques. Sample morphology and elemental composition were analysed on a JEOL JSM-5400 scanning electron microscope using wolfram as the electron source. The microscope was coupled to an Oxford Link ISIS Si/Li energy dispersive X-ray spectrometer. The samples were placed on metallic holders and carbon-coated.

3. Results

3.1. Strength

The experimental conditions for alkaline activation as well as the bending and compressive strength values obtained for the blends are summarised in Table 2. According to these findings, 2-day mechanical strength was higher in blend M1, in particular $M1_{NH}$, with values of up to 23 MPa. In contrast, regardless of the alkaline activator used, blend M2 ($M2_{NS}$ and $M2_{NH}$) exhibited very low strength (under 3 MPa). This may have been partially due to the high *L/S* ratio used to prepare the M2 pastes, as well as to the low density and reactivity of diatomite, as discussed later.

3.2. XRD

The XRD findings are shown in Fig. 1. Most of the reflections on the anhydrous CAC pattern were generated by monocalcium aluminate. The halo from 22° to 38° on the diffractogram for slag is a proof that it consisted primarily of a vitreous phase. The reflections on the diatomite diffractogram, in turn, denote the presence of crystalline phases such as quartz, albite, muscovite and calcite. The new reflections that appeared on the XRD patterns after activation varied with the starting blend (M1 or M2) and the activator used.

In the presence of sodium sulphate (sample $M1_{NS}$), the phases detected were bayerite, ettringite and a phase, whose composition is $3CaO \cdot Al_2O_3 \cdot CaSO_4 \cdot 0.5Na_2SO_4 \cdot 15H_2O$. This compound, known as the U phase (which is an AFm type phase structurally similar to a calcium monosulfoaluminate), was first defined by Dosch et al. [38] and subsequently mentioned in papers by Li et al. [39]. Generally speaking, all these crystalline phases can be associated with the reaction between the CAC and the sodium sulphate, for under these conditions the reaction between the slag and the activator apparently yielded no XRD-detectable crystalline compounds. The main reaction product when M1 was hydrated with the 8-M NaOH solution was katoite, a crystalline phase observed by other authors studying CAC and C_3A hydration at high alkaline concentrations [36]. Here hydrotalcite (phase associated with the slag reaction) was also detected, along with calcium carboaluminate (C_4AcH_{11}), whose presence may have been the result of either the reaction between the CAC and the highly alkaline medium [36] or to slag hydration [23].

In the presence of sodium sulphate ($M2_{NS}$), the new crystalline phases (not identified prior to hydration) found in M2 included bayerite, ettringite and phase U. As noted earlier, these phases were essentially the result of the reaction between the CAC and sodium sulphate. No diffraction lines denoting the formation of new crystalline phases were observed on the diffractogram for sample $M2_{NH}$, either. Although the alkalinity generated was similar in pastes $M1_{NH}$ and $M2_{NH}$, no katoite was detected in the latter.

In addition, the amorphous halo attributed to the starting materials ($2\theta = 20–30°$) shifted to higher two theta values in the patterns for the activated materials, as shown in the diffractograms in Fig. 1. Shift span and intensity varied with the material and activator. Generally speaking, both were much greater in the blends containing slag activated at high alkalinity. In any event, this shift was attributable in all cases to the formation of an XRD-amorphous gel. In light of the chemical composition of the starting materials, this gel may be assumed to be a calcium aluminosilicate or calcium–sodium hydrate.

3.3. NMR

The ^{27}Al MAS-NMR spectra for both the starting materials and the hydration products obtained by hydrating the working blends are shown in Fig. 2. The most prominent characteristic of the CAC spectrum, a wide, intense, asymmetric signal at 78 ppm, was associated with the presence of tetrahedral aluminium (Al_T) [40–43]. Its asymmetry denotes the existence of overlapping components with similar chemical shift values. In a more detailed analysis of the deconvolution of the central signal on the ^{27}Al MAS-NMR spectrum for $CaAl_2O_4$, Pena et al. [43] observed two components with similar symmetries located at +83.5 and +80 ppm. The same spectrum exhibited

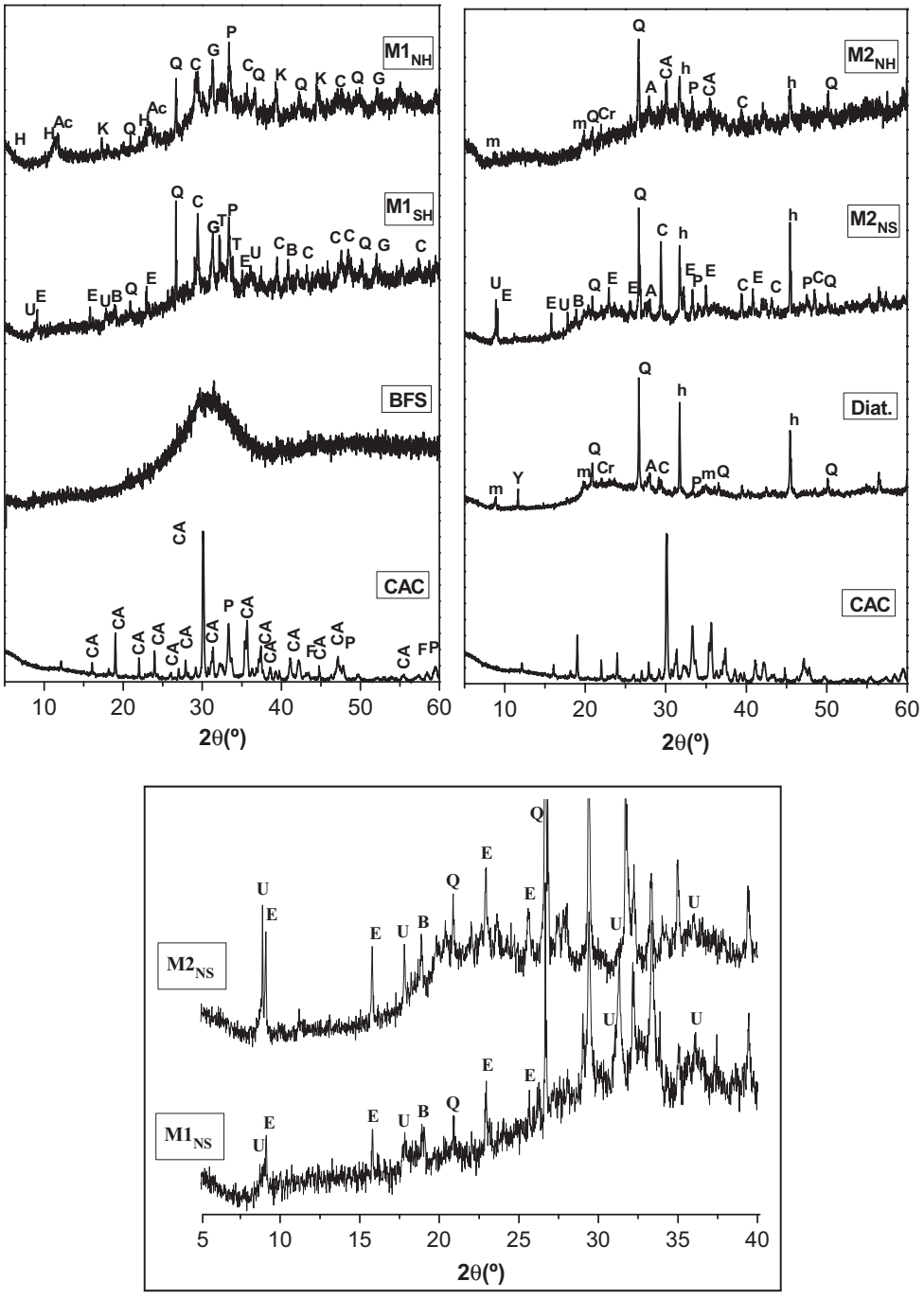

Fig. 1. XRD of the prime materials and 2-day hydrated blends; the reflections characteristic of ettringite and phase U (blends $M1_{NS}$ and $M2_{NS}$) are shown in the lower diffractogram. *Legend*: A = albite (76-758), Ac = C_4AcH_{11} (41-219), B = bayerite (83-2256), C = calcite (86-2339), CA = calcium aluminate (70-134), Cr = cristobalite (39-1425), E = ettringite (72-646), F = Fe_2O_3 (85-1436), G = gehlenite (72-2128), H = hydrotalcite (41-1428), h = halite (05-628), K = katoite (24-217), m = muscovite (80-742), P = perovskite (75-2100), Q = quartz (79-1910), T = thenardite (37-1465), U = $3CaO \cdot Al_2O_3 \cdot CaSO_4 \cdot 0.5Na_2SO_4 \cdot 15H_2O$ (44-272), and Y = gypsum (33-311).

a low intensity signal at 10 ppm, associated with the presence of octahedral aluminium (Al_O) [41–43]. This signal may be related to the formation of a small amount of CAH_{10}, which would be an indication that the CAC was slightly weathered [40].

The single wide signal at +58 ppm on the blast furnace slag spectrum was associated with the (primarily network-forming) Al_T in the vitreous phase of the slag [32,33]. While the diatomite was observed to have a low Al content (4.94% Al_2O_3, as shown in Table 1), its ^{27}Al MAS-NMR spectrum contained a high quality Al signal. The spectrum exhibited two signals with similar intensities at approximately +3 and +56 ppm, an indication that in diatomite the Al was found as both Al_T (+56 ppm) and Al_O (+3 ppm).

In the presence of Na_2SO_4, the ^{27}Al NMR spectra for the two blends ($M1_{NS}$, $M2_{NS}$) had two signals with varying

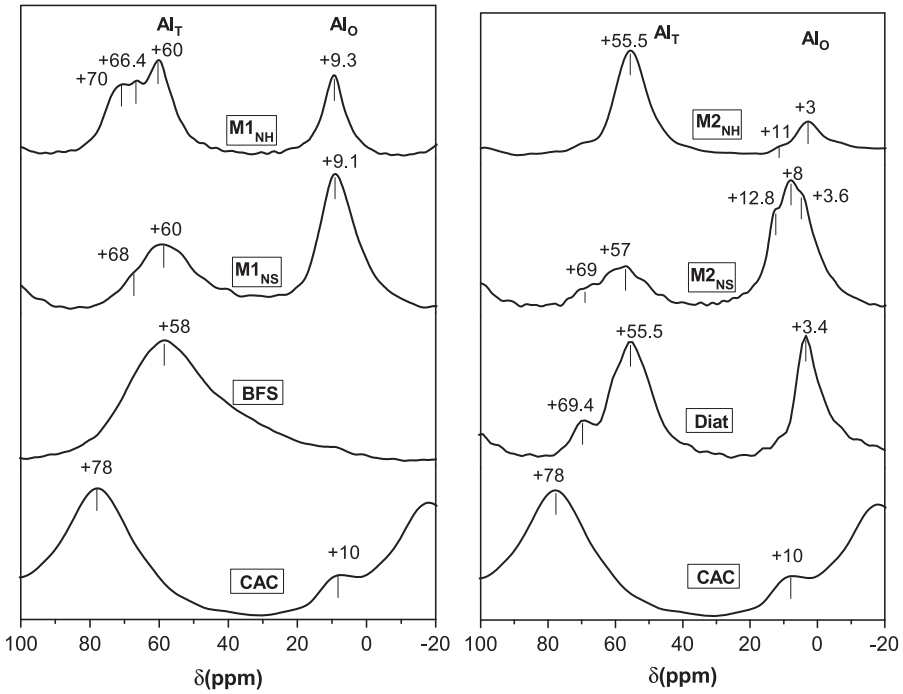

Fig. 2. ^{27}Al MAS-NMR spectra for the starting materials and 2-day hydrated blends.

intensities. The resolution for the most intense, associated with Al_O, was better in blend $M2_{NS}$ (80% diatomite) than in $M1_{NS}$ (80% slag). In the M1 blend, only one asymmetric and wide signal is observed near +9 ppm; however in the M2 blend at least three signals can be distinguished at around +3.5, +8 and +13 ppm. According to previously reported results, the signal around +13 ppm could be associated with the formation of ettringite [44] and the signal near +8/+9 ppm may be attributable to octahedral aluminium in one of CAC hydration phase, probably AH_3 and/or CAH_{10} [40–43]. The signal observed at +3.5 ppm may correspond to Al_O present in the cristaline albite/muscovite phases of the diatomite. While the XRD data confirm the formation of ettringite and U phase in both blends, it is hard to identify the Al_O NMR signals of these phases (+13.2 for ettringite and +10.6 for the U phase [40]) due to the overlap of many signals mostly in M1 blend.

The low intensity signal between +50 and +70 ppm appears to be the outer profile of two narrower signals whose chemical shift values at +60 and +70 ppm denote Al in q^4 (4Si) and q^2 (2Si) environments, respectively [32].

The ^{27}Al NMR spectra for the blends activated with 8-M NaOH solution ($M1_{NH}$, $M2_{NH}$) exhibited very different signal intensities, although the Al_T signal was less intense than the Al_O signal in both cases. On the $M1_{NH}$ spectrum, the signal at 9 ppm may be a combination of several parts, generated by the phases deriving from CAC hydration, probably hydrotalcite and/or katoite phases [43] already detected by XRD. The weak Al_O signal at +3 ppm on the $M2_{NH}$ spectrum may be attributable to the Al_O in the diatomite. No new Al_O-containing phases, or very small amounts of such compounds, appeared to form in this blend. The Al_T signal in the $M2_{NH}$ blend was located at +55 ppm (q^4 environment). Three narrow signals can be distinguished in blend $M1_{NH}$, at +60, +66.4 and +70 ppm, attributed to q^4 (4Si), q^3 (3Si) and q^2 (2Si) environments, respectively [22–24].

The ^{29}Si MAS-NM spectra for the blends and starting materials are shown in Fig. 3. Since CAC has a practically negligible Si content, its spectrum is not reproduced in this figure. The spectrum for slag exhibited a wide signal at around −77 ppm, indicating that the respective silicates were arranged into dimers (Q^1 environments). The diatomite spectrum had three signals with chemical shifts at around −86, −95 and −110 ppm, respectively corresponding to Q^2, Q^3 and Q^4 environments.

The main signals on the spectrum for material $M1_{NS}$ were located at −74.5 ppm (Q^1 environment), a less intense signal at −84.5 ppm (Q^2 environment) and a shoulder at −96.5 ppm. The ^{29}Si spectrum for material $M2_{NS}$ was practically the same as the spectrum for the starting diatomite, perhaps another indication of low diatomite reactivity under these conditions. The width of the signals and their poor resolution may be due to the existence of weakly defined environments or signal overlapping.

As the system alkalinity rose (due to hydration with NaOH), the intensity of the signal associated with slag on the ^{29}Si spectrum for blend $M1_{NH}$ declined substantially, and new signals appeared at −81.8, −85, −88 and −93.2 ppm associated with environments Q^2(1Al), Q^2(0Al), Q^3(3Al) and Q^3(2Al), respectively [22–24]. The spectrum for blend $M2_{NH}$ contained a new signal at around −89 ppm and showed a significant decline in the intensity of the signal at −110 ppm.

4. Discussion

The alkaline activation of two cementitious blends, M1 (20% CAC+80% slag) and M2 (20% CAC+80% diatomite) with two activators (NS and NH) was studied with XRD and NMR to ascertain the activation mechanisms triggered by each

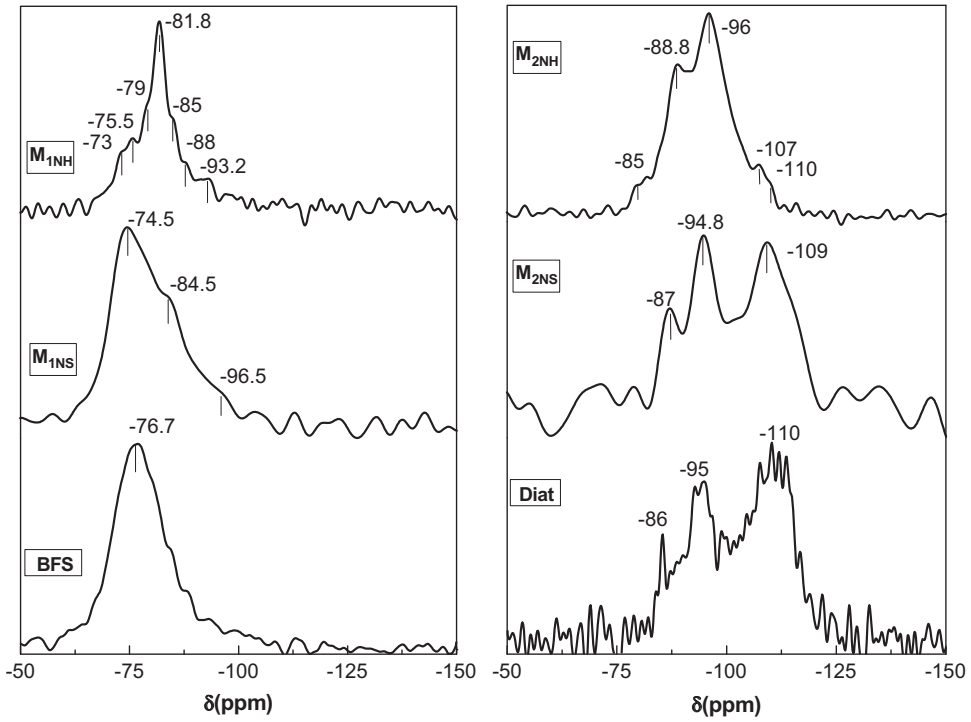

Fig. 3. ^{29}Si MAS-NMR spectra for the starting materials and 2-day hydrated blends.

activator and identify the reaction products formed. During alkaline activation, all the starting materials in the two blends, including the alkaline activator, participated in the formation of the final material, with the CAC furnishing Al and Ca; the slag mainly Si and Ca; the diatomite Si; and the activators, alkalis and sulphates. The cementitious properties of the end products were normally related to the formation of gels whose nature (C–A–S–H- or (N,C)–A–S–H-like) depended on the prime materials and activator used.

4.1. Activation with Na_2SO_4

When Na_2SO_4 was used as the activator, two calcium sulphoaluminate hydrates, ettringite and phase U, were observed to form in both $M1_{NS}$ and $M2_{NS}$. As previously described by Scrivener [45], the equation for ettringite formation from CA and gypsum can be written as

$$3(CaO \cdot Al_2O_3) + 3(\underset{\text{Gypsum}}{CaSO_4 \cdot xH_2O}) + (38-3x)H_2O \rightarrow \underset{\text{Ettringite}}{(CaO)_6(Al_2O_3)(SO_3)_3 \cdot 32H_2O} + 2(Al_2O_3 \cdot 3H_2O) \quad (1)$$

In our case where CAC is hydrated in the presence of sodium sulphate (Na_2SO_4) instead of gypsum, the equation for ettringite formation takes the form as depicted below:

$$6(CaO \cdot Al_2O_3) + \underset{\text{Sodiumsulphate}}{Na_2SO_4} + 48H_2O \rightarrow \underset{\text{Ettringite}}{(CaO)_6(Al_2O_3)(SO_3)_3 \cdot 32H_2O} + 5(Al_2O_3 \cdot 3H_2O) + 2(Na^+, OH^-) \quad (2)$$

This reaction raised system pH by releasing alkalis, which in turn had a dual effect on the subsequent reactions. On the one hand, the slag dissolved more readily, prompting the early participation of its majority elements (essentially Si, Ca and Al) in C–A–S–H gel formation. On the other, higher pH favoured the formation of phase U ($3CaO \cdot Al_2O_3 \cdot CaSO_4 \cdot 0.5Na_2SO_4 \cdot 15H_2O$). Indeed, the presence of phase U (detected by XRD) confirmed the rise in pH, which forms only in the presence of alkalis. Some authors believe that this phase is the result of ettringite conversion in highly alkaline media [38,39,44]. In the present study, the co-existence of phase U and ettringite may be related to the reversible nature of that conversion. A more likely explanation, however, is that the system pH climbed transiently to a high value, but not long enough for total ettringite conversion. The inference is that either the alkali concentration in the medium was not high enough for full transformation or, more probably, the alkalis were taken up in an (N,C)–A–S–H-like gel to neutralise charges, lowering the pH and reversing the process. Some authors [38,39] have observed the presence of intermediate products (such as C_4AH_{13} or AFm) during AFt→phase U conversion. In a prior study, Sánchez-Herrero et al. [46] reported that C_4AH_{13} formation is not necessarily an intermediate stage in AFt→phase U conversion, but may be regarded as a hydration product that forms when calcium sulphoaluminate undergoes conversion.

An NMR study of ettringite stability in alkaline solutions at 80 °C showed that phase U appeared as a signal at around +10.6 ppm on the ^{27}Al spectrum, while the signal associated with ettringite was located at around +13.2 ppm [44]. In the present study, the signal associated with Al_O in both $M1_{NS}$ and $M2_{NS}$ was wide and asymmetric and sprawled across approximately 30 ppm (from 20 to −10 ppm) spectral interval. This made it difficult to distinguishamong the signals for ettringite,

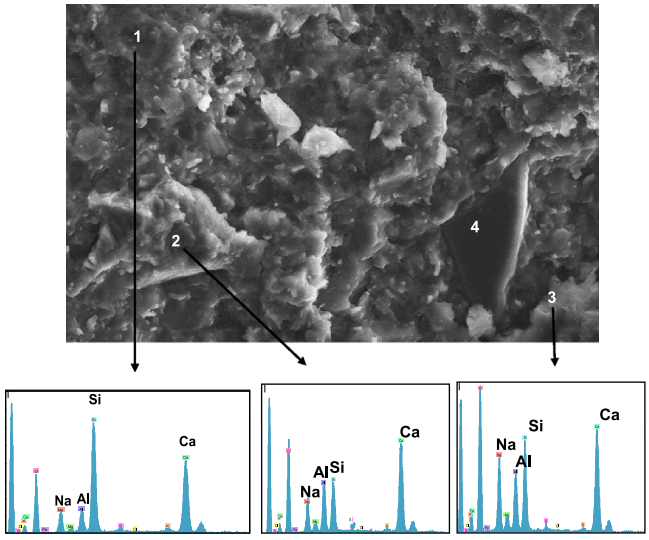

Fig. 4. SEM image of sample $M1_{NH}$ and EDX spectra for the areas indicated; region 4 constitutes an unreacted BFS particle.

phase U and any possibly overlapping signals associated with the products of CAC hydration, although thanks to the somewhat better resolution in blend $M2_{NS}$, the signal at +3.6 ppm could be attributed to the Al_O in the diatomite, the signal at around +8 ppm to bayerite and the signal at around +12.8 ppm to the Al_O in the ettringite and/or phase U.

Further to the XRD and NMR findings, in the presence of sodium sulphate ($M1_{NS}$, $M2_{NS}$), diatomite barely reacted and the scant mechanical strength developed by the end material was due essentially to the fact that the sulphoaluminates deriving from CAC hydration (ettringite and phase U) enhanced matrix density. In blend $M1_{NS}$, the slag obviously reacted with some intensity (much greater than that of the diatomite in blend $M2_{NS}$), enabling the material to develop acceptable mechanical strength (10.7 MPa). All the foregoing were very likely due to the formation of a cementitious gel with apparently high percentages of Q^2 units: in other words, this gel was probably a C–(A)–S–H-like substance with a small amount of aluminium in its structure.

4.2. Activation with NaOH

In the blends activated with caustic soda ($M1_{NH}$ and $M2_{NH}$), both the slag and the diatomite reacted much more intensely than when the activator was Na_2SO_4 (see Fig. 3). This was primarily due to a substantial rise in system pH, which enhanced the solubility of both prime materials.

The slag in paste $M1_{NH}$ reacted at such high alkalinity as per mechanisms described previously [22,23] to generate a C–A–S–H-like gel, while the CAC yielded carboaluminates and calcium aluminate hydrates (see Fig. 1). Another significant finding in connexion with the reaction products identified was that the high system pH not only favoured but also accelerated the formation of cubic hydrates (C_3AH_6), an indication that metastable hexagonal aluminates had already converted to cubic compounds in the 2-day material. This process can take years in water-hydrated CAC. Similar findings were observed when CAC behaviour was studied in the presence of high alkaline concentrations in the absence of soluble silica [37]. The interaction between the silicate ions in the slag and the Al ions in the CAC was apparently weak under these conditions. Nonetheless, the NMR findings showed that while the two materials interacted only scantily, some degree of synergy or interaction between the slag and the CAC did appear to be present when system alkalinity was high.

Three environments for tetrahedral Al were observed on the ^{27}Al spectrum for $M1_{NH}$, at positions +70, +66.4 and +60 ppm (Fig. 2). Normally the Al_T in slag alkali-activated with NaOH [22,23] generates a sole signal at +70 ppm (aluminium in the bridging position in a linear silicate chain), denoted by the presence of $Q^2(1Al)$ signals on ^{29}Si MAS-NMR spectra. The presence of this signal in the present study confirmed the existence of a C–A–S–H gel [24]. The signals at +66.4 and +60 ppm indicated a high rate of replacement of Si by Al tetrahedra, in turn confirmed by the presence of $Q^3(n\mathrm{Al})$ environments (signals at around 88 and 93 ppm on the ^{29}Si spectrum in Fig. 3). These findings showed that the structure of the C–A–S–H gel formed was two-dimensional and that the CAC and slag were interacting to some extent.

Additionally by means of scanning electron microscopy it has been proved that the 2-day $M1_{NH}$ paste was a compact material including particles with a composition typical of a C–A–S–H gel (point 1), together with others with a higher Ca and Al content (points 2 and 3), possibly resulting from the uptake of Ca and Al released by the CAC. The presence of anhydrous slag particles (point 4) showed that some of the material was yet to react in the 2-day samples. The EDX spectra in Fig. 4 denote the presence of significant amounts of Na in the gels. This sodium was taken up in the gel structure to neutralise the charge generated when a Si tetrahedron is replaced by an Al tetrahedron. These findings and the authors' interpretations confirm the NMR results discussed above and reveal the existence of some synergies between the materials comprising blend M1 in high alkalinity conditions. The CAC furnishes Al and possibly Ca, interacting with the slag. The CAC hydrates and slag together form an Al-rich gel whose two-dimensional structure affords the hardened material its mechanical properties (~23 MPa).

The XRD findings for blend $M2_{NH}$, in turn, showed that in contrast to what was observed in blend $M1_{NH}$, the hydrates normally appearing in CAC hydration did not precipitate and part of this material had not yet reacted. While according to the ^{29}Si NMR findings (Fig. 3), diatomite reactivity rose steeply in the presence of caustic soda, the mechanical tests showed that material strength remained very low despite the higher reactivity with NaOH than with sodium sulphate.

The non-formation of CAC hydrates at high pH in the presence of an additional source of silica, in turn, was observed in a prior study [47]. In CAC+sodium silicate blends [37], while a small amount of katoite was detected in 2-day samples, this phase was absent in the 28-day material, where a calcium aluminosilicate hydrate appeared. The NMR findings confirmed the hypothesis that in blend $M2_{NH}$, the interaction between the silica in the diatomite and the aluminium and

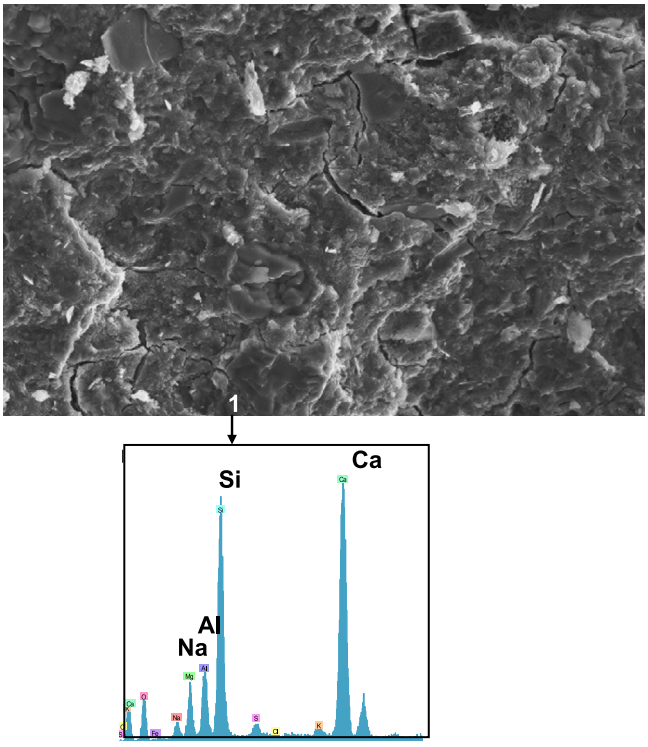

Fig. 5. SEM image of sample $M2_{NH}$ and EDX spectra for the areas indicated.

calcium in the CAC yielded a calcium aluminosilicate hydrate not detectable by XRD due, in all likelihood, to its disorderly structure. In contrast, the very small amount of octahedral Al identified on the ^{27}Al MAS-NMR spectrum for material $M2_{NS}$ (see Fig. 2) clearly showed that no normal CAC hydrates formed in this blend. Large amounts of tetrahedral aluminium were present at +55 ppm, however, and attributed to Al-Q^4(4Si) units [37], which are distinctly different from the Al_T present in the anhydrous CAC with a signal at +78 ppm. While the ^{27}Al spectrum for diatomite exhibited a certain amount of Al_T at +55 ppm, it could hardly be attributed to unreacted diatomite alone, given the high intensity of that signal on the sample $M2_{NH}$ profile. On the ^{29}Si spectrum, in turn, the wide, intense signal between −87 and −89 ppm was similar to the signal reported in the studies mentioned above on CAC+Mk+8-M NaOH [47] and CAC+sodium silicate [37] blends. There it was attributed to the presence of Q^4(4Al) or Q^3(3Al) units associated with the formation of an (N,C)–A–S–H gel-like alkaline aluminosilicate hydrate. Fig. 5 shows that the matrix of this product consisted primarily of a Ca- and Si-rich amorphous material containing Al and some Na in its structure. This finding proves that the CAC clearly interacted with diatomite in blend $M2_{NH}$.

While the degree of reaction between diatomite and CAC was not quantified, both the XRD and NMR findings appear to indicate that it was not very high in the 2-day samples. This, in conjunction with the L/S ratio used to prepare the pastes (ratio required to obtain good workability) and the low density of the resulting material, may largely explain the low mechanical strength developed by blend $M2_{NH}$, despite the CAC–diatomite interaction.

5. Conclusions

The conclusions that can be drawn from the XRD and (^{27}Al and ^{29}Si) NMR characterisation of the products formed during the alkaline activation of blends M1 and M2 with two types of activators are listed below.

- Both the composition of the starting system and the pH of the medium have a considerable impact on the nature and properties of the compounds formed.
- Activating blend M1 in a moderately alkaline medium (generated by Na_2SO_4) yielded a C–(A)–S–H gel and sulphoaluminates (ettringite and phase U), whereas under the same conditions only CAC hydration products (ettringite and phase U) were identified in blend M2, for the diatomite failed to react.
- In a high alkalinity medium (generated by caustic soda), blend M1 activation yielded an (N,C)–A–S–H gel, katoite and carboaluminates (hydrotalcite, C_4AcH_{11}). While diatomite was more reactive at high than at moderate alkalinity, the scant availability of the majority element (Si), together with the low Al and Ca contents in blend M2 hindered the formation of a sufficient amount of cementitious gel to improve the mechanical properties of the final material.

Acknowledgements

This study was funded by the Spanish Ministry of the Economy and Competitive Affairs under Project BIA 2010-17530. K. Arbi worked under a 2009 Post-graduate Studies Council contract, co-funded by the Spanish National Research Council (CSIC) and the European Social Fund.

References

[1] K.L. Scrivener, R.J. Kirkpatrick, Innovation in use and research on cementitious material, Cement and Concrete Research 38 (2008) 128–136.
[2] M.W. Palomo, M.T. Grutzeck, Blanco alkali-activated fly ashes—a cement for the future, Cement and Concrete Research 29 (1999) 1323–1329.
[3] M.L. Granizo, M.T. Blanco-Varela, A. Palomo, Influence of the starting kaolin on alkali-activated materials based on metakaolin. Study of the reaction parameters by isothermal conduction calorimetry, Journal of Materials Science 35 (2000) 6309–6315.
[4] A. Buchwald, H. Hilbig, C.h. Kaps, Alkali-activated metakaolin-slag blends—performance and structure in dependence of their composition, Journal of Materials Science 42 (2007) 3024–3032.
[5] M. Steveson, K. Sagoe-Crentsil, Relationships between composition, structure and strength of inorganic polymers: Part I. Metakaolin-derived inorganic polymers, Journal of Materials Science 40 (2005) 2023–2036.
[6] A. Fernandez-Jimenez, F. Puertas, L. Fernández-Carrasco, Alkaline-sulphate activation processes of a Spanish blast furnace slag, Materiales de Construcción 46 (1996) 23–37.
[7] S.A. Bernal, E.D. Rodriguez, R.M. de Gutierrez, M. Gordillo, J.L. Provis, Mechanical and thermal characterisation of geopolymers based on silicate-activated metakaolin/slag blends, Journal of Materials Science 64 (2011) 5477–5486.
[8] C. Shi, A. Fernández-Jiménez, A. Palomo, New cements for the 21st century: the pursuit of an alternative to Portland cement, Cement and Concrete Research 41 (2011) 750–763.

[9] E. Rodríguez, S.A. Bernal, R.M. de Gutiérrez, F. Puertas, Hormigón alternativo basado en escorias activadas alcalinamente, Materiales de Construcción 58 (2008) 53–67.
[10] J. Deja, Carbonation aspects of alkali activated slag mortars and concretes, Silicates Industriels 67 (2002) 37–42.
[11] V.D. Glukhovskiy, Soil Silicates, Gosstroy Publisher, Kiev, 1959 In Russian.
[12] P.V. Krivenko, G.Yu. Kovalchuk, Fly Ash Based Zeolite Cements. Innovations and Developments in Concrete Materials and Construction, in: Proceedings of the International Conference on Challenges of Concrete Construction, Dundee, 2002, pp. 123–132.
[13] G. Kovalchuk, A. Fernández-Jiménez, A. Palomo, Alkali-activated fly ash. Relationship between mechanical strength gains and initial ash chemistry, Materiales de Construcción 58 (2008) 35–52.
[14] A. Palomo, S. Alonso, A. Fernández-Jiménez, I. Sobrados, J. Sanz, Alkaline activation of fly ashes: NMR study of the reaction products, Journal of the American Ceramic Society 87 (2004) 1141–1145.
[15] A. Fernández-Jiménez, A. Palomo, C. López-Hombrados, Engineering properties of alkali-activated fly ash concrete, ACI Materials Journal 103 (2006) 106–112.
[16] P. Duxson, J.L. Provis, G.C. Lukey, S.W. Mallicoat, W.M. Kriven, J.S.J. van Deventer, Understanding the relationship between geopolymer composition, microstructure and mechanical properties, Colloids and Surfaces A 269 (2005) 47–58.
[17] A. Buchwald, M. Schulz, Alkali-activated binders by use of industrial by-products, Cement and Concrete Research 35 (2005) 968–973.
[18] P. Lemougna, K. MacKenzie, U.F. Chinje Melo, Synthesis and thermal properties of inorganic polymers for structural and refractory applications from volcanic ash, Ceramics International 37 (2011) 3011–3018.
[19] J.G.S. Van Jaarsveld, J.S.J. Van Deventer, Effect of the alkali metal activator on the properties of fly ash-based geopolymers, Industrial and Engineering Chemistry Research 38 (1999) 3932–3941.
[20] H. El-Didamony, A.A. Amer, H. Abd Ela-ziz, Properties and durability of alkali-activated slag pastes immersed in sea water, Ceramics International 38 (2012) 3773–3780.
[21] C. Shi, P.V. Krivenko, D. Roy (Eds.), Taylor & Francis, Abingdon, UK, 2006.
[22] S.D. Wang, K.L. Scrivener, ^{29}Si and ^{27}Al NMR study of alkali-activated slag, Cement and Concrete Research 33 (2003) 769–774.
[23] A. Fernández-Jiménez, F. Puertas, I. Sobrados, J. Sanz, Structure of calcium hidrates formed in alkaline-activated slag: influence of the type of alkaline activator, Journal of the American Ceramic Society 86 (2003) 1389–1394.
[24] F. Puertas, M. Palacios, H. Manzano, J.S. Dolado, A. Rico, J. Rodríguez, A model for the C-A-S-H gel formed in alkali-activated slag cements, Journal of the European Ceramic Society 31 (2011) 2043–2056.
[25] W.-T. Tsai, C.-W. Lai, K.-J. Hsien, Characterization and adsorption properties of diatomaceous earth modified by hydrofluoric acid etching, Journal of Colloid and Interface Science 297 (2006) 749–754.
[26] S. Nenadovic, M. Nenadovic, R. Kovacevic, Lj. Matovic, B. Matovic, Z. Jovanovic, J. Grbovic Novakovic, Influence of diatomite microstructure on its adsorption capacity for Pb(II), Science of Sintering 41 (2009) 309–317.
[27] Z.-Y. Wang, Li-P. Zhang, Yu-X. Yang, Structural investigation of some important Chinese diatomites, Glass Physics and Chemistry 35 (2009) 673–679.
[28] M.I. Al-Wakeel, Characterization and process development of the Nile diatomaceous sediment, International Journal of Mineral Processing 92 (2009) 128–136.
[29] K. Pimraksa, P. Chindaprasirt, Lightweight bricks made of diatomaceous earth, lime and gypsum, Ceramics International 35 (2009) 471–478.
[30] S.A. Miller, A.R. Sakulich, M.W. Barsoum, E. Jud Sierra, Diatomaceous earth as a Pozzolan in the fabrication of an alkali-activated fine-aggregate limestone concrete, Journal of the American Ceramic Society 93 (2010) 2828–2836.
[31] E. Jud Sierra, S.A. Miller, A.R. Sakulich, K. MacKenzie, M.W. Barsoum, Pozzolanic activity of diatomaceous earth, Journal of the American Ceramic Society 93 (2010) 3406–3410.
[32] A. Fernández-Jiménez, A. Palomo, I. Sobrado, J. Sanz, The role played by the reactive alumina content in the alkaline activation of fly ashes, Microporous Mesoporous Materials 91 (2006) 111–119.
[33] P. De Silva, K. Sagoe-Crenstil, V. Sirivivatnanon, Kinetics of geopolymerization: role of Al_2O_3 and SiO_2, Cement and Concrete Research 37 (2007) 512–518.
[34] J.L. Provis, J.S.L. van Deventer, Geopolymers: Structures, Processing, Properties and Industrial Applications, Woodhead Publishing, Abingdon, UK, 2009.
[35] R. Vallepu, A. Fernandez-jimenez, T. Terai, A. Mikuni, A. Palomo, K.J.D. Mackenzie, K. Ikeda, Effect of synthesis pH on the preparation and properties of K–Al-bearing silicate gels from solution, Journal of the Ceramic Society of Japan 114 (2006) 624–629.
[36] C. Pastor, A. Fernandez-Jimenez, T. Vazquez, A. Palomo, Calcium aluminate cement hydration in a high alkalinity environment, Materiales de Construcción 59 (2009) 21–34.
[37] A. Fernández-Jiménez, T. Vazquez, A. Palomo, Effect of sodium silicate on calcium aluminate cement hydration in highly alkaline media: a microstructural characterization, Journal of the American Ceramic Society 94 (2011) 1297–1303.
[38] W. Dosch, H. zur Strassen, Ein alkalihaltiges calciumaluminatsulfathydrat, Zement Kalk Gips 20 (1967) 392–401.
[39] G. Li, P. Le Bescop, M. Moranville, The U phase formation in cement-based systems containing high amounts of Na_2SO_4, Cement and Concrete Research 26 (1) (1996) 27–33.
[40] X.D. Cong, R.J. Kirkpatrick, Hydration of calcium aluminate cements—a solid-state Al-27 NMR-study, Journal of the American Ceramic Society 76 (1993) 409–416.
[41] D. Muller, W. Gessner, A. Samoson, E. Lippmaan, Solid-state Al-27 NMR-studies on polycrystalline aluminates of the system $CaO–Al_2O_3$, Polyhedron 5 (1986) 779–785.
[42] J. Skibsted, E. Henderson, H.J. Jakobsen, Characterization of calcium aluminate phases in cements by Al-27 MAS NMR-spectroscopy, Inorganic Chemistry 32 (1993) 1013–1027.
[43] P. Pena, J.M. RivasMercury, A.H. de Aza, X. Turrillas, I. Sobrados, J. Sanz, Solid-state Al-27 and Si-29 NMR characterization of hydrates formed in calcium aluminate-silica fume mixtures, Journal of Solid State Chemistry 181 (2008) 1744–1752.
[44] Y. Shimada, J.F. Young, Thermal stability of ettringite in alkaline solutions at 80 °C, Cement and Concrete Research 34 (2004) 2261–2268.
[45] K.L. Scrivener, Calcium aluminate cements, in: J. Newman, B.S. Choo (Eds.), Advanced Concrete Technology: Constituent Materials, Elsevier Butterworth-Heinemann, Oxford, UK, 2003, pp. 2/1–2/28.
[46] M.J. Sanchez-Herrero, A. Fernández-Jiménez, A. Palomo, Alkaline hydration of tricalcium aluminate, Journal of Ceramic Society 95 (2012) 3317–3324.
[47] A. Fernández-Jiménez, A. Palomo, T. Vazquez, R. Vallepu, T. Terai, K. Ikeda, Alkaline activation of blends of metakaolin and calcium aluminate, Journal of the American Ceramic Society 91 (2008) 1231–1236.